Available online at www.sciencedirect.com
ScienceDirect
Applied Catalysis A: General 319 (2007) 38–46
APPLIED CATALYSIS A: GENERAL
www.elsevier.com/locate/apcata

# Production of ultrapure hydrogen in a Pd–Ag membrane reactor using $Ru/La_2O_3$ catalysts

B. Faroldi, C. Carrara, E.A. Lombardo, L.M. Cornaglia *

*Instituto de Investigaciones en Catálisis y Petroquímica (FIQ, UNL-CONICET), Santiago del Estero, 2829-3000 Santa Fe, Argentina*

Received 7 August 2006; received in revised form 5 November 2006; accepted 11 November 2006
Available online 12 December 2006

**Abstract**

Ru catalysts supported on lanthanum oxide with different loadings were prepared by wet impregnation. These solids were characterized by laser Raman spectroscopy (LSR), XPS, XRD and TPR. The catalytic activity toward hydrogen production through the dry reforming of methane was determined in a fixed-bed reactor and a membrane reactor. The reaction rate expressed per gram of Ru decreased when the metal loading increased.

In the Pd–Ag membrane reactor, when the sweep gas flow rate (SG) increased, the conversions overcame the equilibrium values and the difference between $CH_4$ and $CO_2$ conversions decreased. Both Ru(0.6) and Ru(1.2) catalysts were able to restore the equilibrium for the dry reforming reaction up to values of SG = 30 ml $min^{-1}$; Ru(0.6) was the most effective catalyst. By employing a $CO_2/CH_4 = 1$ and a SG of 0.05 mmol $s^{-1}$, both a high $H_2$ permeation flux of $5.68 \times 10^{-7}$ mol $s^{-1}$ $m^{-2}$ and a hydrogen recovery of 80% were obtained.

Both the TPR and the Raman spectroscopy data indicated the presence of Ru(III) strongly interacting with La. Significantly, this observation was further confirmed by the appearance of Ru(III) on the surface. When the Ru content increased, the higher Ru 3d binding energy component was proposed as arising from Ru(IV). Concerning the Ru(1.2) solid, the presence of Ru(IV) was detected by means of TPR experiments, in agreement with the high proportion of Ru(IV) on the surface. Therefore, a fraction of Ru loading was present in this solid as species with weaker metal–support interaction leading to the slight deactivation of this catalyst in the membrane reactor.


*Keywords:* Membrane reactor; Hydrogen production; $Ru/La_2O_3$; $CO_2$ reforming

## 1. Introduction

Catalytic dry reforming is the reaction of carbon dioxide with methane to produce syngas. If the main goal is to produce $H_2$, this reaction can be carried out in two different ways: in a fixed-bed reactor followed by the purification steps, or in a membrane reactor combining the reaction and the purification in a single vessel. In the latter option, the system offers the possibility of overcoming the thermodynamic limitations of this endothermic reaction, allowing the attainment of higher methane conversions at lower temperatures.

Recently, several studies [1–7] related to the application of membrane reactors to this reaction have achieved higher conversions with respect to a conventional fixed-bed reactor. Moreover, dense Pd/Ag membranes exhibit almost 100% selectivity toward hydrogen, so that ultrapure hydrogen could be produced. To optimize the membrane reactor operation, a balance between the hydrogen produced and the hydrogen removed is a necessary condition [8].

For dehydrogenation reactions carried out in membrane reactors, Dalmon and co-workers [9] sustained that the problem of the catalysts may be non-trivial; however, this topic has been underestimated in the recent literature. In most cases, a suitable catalyst has to be designed.

Previous studies in fixed-bed reactors [10] have shown that noble metals like rhodium and ruthenium are more active than Ni for the methane reforming reactions. Furthermore, when the appropriate supports are used these formulations are catalytically stable and do not produce a significant amount of carbonaceous residues. Ruthenium, which has applications in several hydrogen-producing reactions, has been selected as an active element due to its relative low price compared with Rh.

The activity and selectivity of Ru catalysts depend greatly on the oxidation state [10] of the metal, which can change

* Corresponding author. Tel.: +54 342 4536861; fax: +54 342 4536861.
*E-mail address:* lmcornag@fiqus.unl.edu.ar (L.M. Cornaglia).

0926-860X/$ – see front matter 
doi:10.1016/j.apcata.2006.11.015

depending on the reaction conditions and the support used. Besides, the support can have a great influence on the type of carbonaceous species formed during reaction.

Support effects on the catalytic behavior of Ru catalysts were investigated by Nagaoka et al. [11]. The activity order of the solids was in agreement with the basicity of the support, indicating that the $CO_2$ adsorption ability (as carbonate type species) on the supports determines the catalytic activity. However, Mark and Maier [12] observed no effect of the support on the reaction rate and Ferreira-Aparicio et al. [13] found an active role of the support in $Ru/SiO_2$ to $Ru/Al_2O_3$, and proposed different reaction mechanisms for each catalyst.

In La-containing Rh catalysts, a high stability has been reported [7,14] in fixed-bed reactors attributed to the metal–support interaction. For $Rh/La_2O_3$ solids, this interaction was very strong. However, when a composite $La_2O_3$-$SiO_2$ material was used as support, a weaker interaction was observed.

In a previous work, we adopted the reaction equilibration ratio ($\eta = p_{CO}^2 p_{H_2}^2 / p_{CH_4} p_{CO_2} K_{eq}$) to compare the behavior of different Rh catalysts in a membrane reactor. This ratio was defined for the carbon dioxide reforming reaction ($CH_4 + CO_2 \leftrightarrow 2CO + 2H_2$). The best performing formulation was obtained using the composite $La_2O_3$-$SiO_2$ support. For this catalyst, the reaction equilibration ratio remained constant and close to 1 with the increase of the sweep gas flow when an appropriate W/F was applied, indicating that the $Rh/La_2O_3$-$SiO_2$ catalyst was able to restore the equilibrium.

The purpose of this work was to develop low-loading $Ru/La_2O_3$ catalyts to be applied in membrane reactors for ultrapure hydrogen production. The catalytic activity toward hydrogen production was determined in both a fixed-bed reactor and a membrane reactor. The reaction equilibration ratio was applied in order to evaluate the catalytic behavior of the Ru catalyts in the membrane reactor. The solids were characterized by laser Raman spectroscopy (LSR), XPS, XRD and TPR. The different behavior was discussed taking into account the characterization results.

## 2. Experimental

### 2.1. Catalyst preparation

The $Ru/La_2O_3$ catalysts were prepared by the conventional wet impregnation of $RuCl_3 \cdot 3H_2O$ onto $La_2O_3$ (Anedra 99.99%). The amount of hydration water in the $RuCl_3$ was determined by thermogravimetric analysis. The impregnated solids were then heated at 353 K to evaporate the water, and dried at 383 K overnight. The catalysts were calcined for 6 h at 823 K in flowing air and then reduced at 823 K in $H_2$ flow for 2 h. The same preparation method was employed to obtain the $Ru/Al_2O_3$ sample.

### 2.2. Catalyst characterization

#### 2.2.1. Metal dispersion

The Ru dispersion of the fresh catalyst, following the hydrogen reduction at 823 K for 2 h, was determined by the static equilibrium adsorption of $H_2$ or CO at 373 K in a conventional vacuum system.

#### 2.2.2. X-ray photoelectron spectroscopy (XPS)

The XPS measurements were carried out using an Axis Ultra Kratos electron spectrometer. Non-monochromatic Mg Kα X-ray radiation was used (10 kV, 15 mA). The pressure in the analysis chamber was about $1 \times 10^{-7}$ Pa during spectra collection. The XPS analyses were performed on the used catalyst and on the calcined solids before and after treatment with hydrogen. The spectral regions corresponding to La 3d, C 1s, O 1s, Ru 3d and Ru 3p core levels were recorded for each sample.

#### 2.2.3. Laser Raman spectroscopy

The Raman spectra were recorded with a TRS-600-SZ-P Jasco Laser Raman instrument, equipped with a charge coupled device (CCD) with the detector cooled to about 153 K using liquid $N_2$. The excitation source was the 514.5 nm line of a Spectra 9000 Photometrics Ar ion laser. The laser power was set at 30 mW.

#### 2.2.4. X-ray diffraction (XRD)

The XRD patterns of the calcined and used solids were obtained with an XD-D1 Shimadzu instrument, using Cu Kα radiation at 30 kV and 40 mA. The scan rate was $1.0^\circ$ $min^{-1}$ for values between $2\theta = 10^\circ$ and $70^\circ$.

#### 2.2.5. Temperature-programmed reduction (TPR)

An Ohkura TP-20022S instrument equipped with a TCD was used for the TPR experiments. To eliminate the carbonates present in the samples, the following pretreatment was used: the samples were heated up to 823 K in oxygen flow, kept constant for 1 h and then cooled down in Ar flow. Afterwards, they were reduced in a $5\%H_2$–Ar stream, with a heating rate of 10 K/min up to the maximum treatment temperature.

### 2.3. Catalytic test

#### 2.3.1. Fixed-bed reactor

The catalyst (50 mg) was loaded into a tubular quartz reactor (inner diameter, 5 mm) which was placed in an electric oven. A thermocouple in a quartz sleeve was placed on top of the catalyst bed. The catalysts were heated in Ar at 823 K and then reduced in situ in flowing $H_2$ at the same temperature for 2 h. After reduction, the temperature was adjusted in flowing Ar to the reaction temperature (823 K); and the feed gas mixture (33%$CH_4$ v/v, 33% $CO_2$, 34% Ar, $W/F = 4.3 \times 10^{-6}$ g h $ml^{-1}$, $P = 1$ atm) was switched to the reactor always kept at 823 K. The stability tests were carried out at $W/F = 2.67 \times 10^{-5}$ g h $ml^{-1}$; conversion was measured at $W/F = 4.3 \times 10^{-6}$ g h $ml^{-1}$. The reaction products were analyzed in a TCD gas chromatograph (Shimadzu GC-8A) equipped with a Porapak column, and a molecular sieve column.

#### 2.3.2. Membrane reactor

The double tubular membrane reactor was built using a commercial dense Pd–Ag alloy (inner tube), provided by

REB Research and Consulting, with one end closed and an inner tube to allow Ar sweep gas flow rate (SG). The permeation area was approximately 5 $cm^2$ (thickness = 50 μm). The outer tube was made of commercial non-porous quartz (i.d. 9 mm). The catalyst (1 g), diluted with quartz chips (2 g), was packed in the outer annular region (shell side). The inner side of the membrane in all runs was kept at atmospheric pressure. More details have been previously reported [7]. The catalysts pretreatment was the same as for the fixed bed reactor. Afterwards, the feed stream gas mixture (33%$CH_4$ v/v, 33% $CO_2$, 34% He, $P$ = 1 atm, W/F = $1.03 \times 10^{-3}$ g h $ml^{-1}$) was switched through the reactor.

In order to measure the equilibrium conversions, the membrane reactor was operated with neither sweep gas nor pressure difference between the tube and the shell sides. The conversions were measured after a 12-h stabilization period. The reaction products and the permeated mixture were analyzed with a TCD gas chromatograph equipped with a Porapak and a molecular sieve column and with an on-line Balzers Quadstar TU 422 quadrupole mass spectrometer previously calibrated for each gas. The carbon balance was close to one in all cases.

## 3. Results and discussion

### 3.1. Fixed-bed reactor measurements

The catalytic activity of Ru catalysts with different metal contents is shown in Table 1. The experiments were carried out at 823 K. This temperature is 50 K below the maximum value allowed for the Pd–Ag membrane when exposed to a reducing atmosphere. It can be observed that the reaction rate expressed per gram of catalyst increases with the Ru content. However, the rate expressed per gram of Ru decreases when the metal loading increases. The reaction rate has been normalized per gram of metal due to uncertainties in determining the metal surface area in the presence of the decorating support [15].

In the fixed-bed reactor, the $CO_2$ conversion was higher than the $CH_4$ conversion due to the occurrence of the RWGS reaction in which $CO_2$ reacted with the $H_2$ produced in the reforming reaction.

$$CH_4 + CO_2 \leftrightarrow 2CO + 2H_2$$

$$H_2 + CO_2 \leftrightarrow CO + H_2O$$

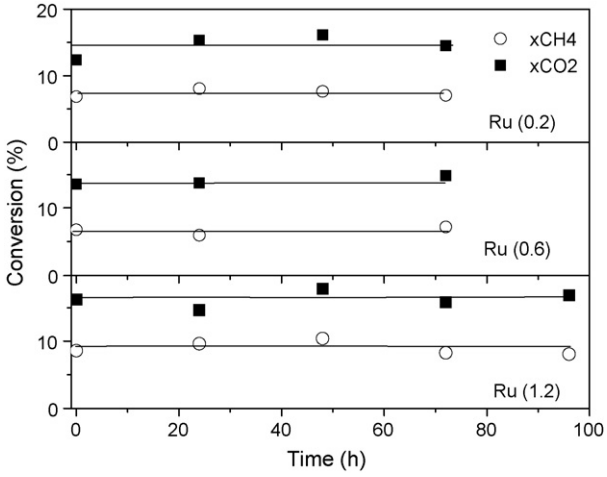


Fig. 1. Stability test of the catalysts in fixed-bed reactor ($T$ = 823 K, W/F = $4.3 \times 10^{-6}$ g h $ml^{-1}$).

The stability of the catalysts in a fixed-bed reactor is presented in Fig. 1. All solids remained stable for more than 70 h in reaction.

Several studies [16–18] have shown the high activity of Ru supported and exchanged catalysts. Bradford and Vannice [17] compared high dispersion catalysts (>50%) and found that the turnover frequencies decreased in the order $TiO_2$ > Alumina ≫ C. They emphasized the need to work at low conversion relative to equilibrium condition in order to obtain accurate kinetic data. On the other hand, Wei and Iglesia [18] reported that forward turnover rates were strongly influenced by Ru dispersion but essentially insensitive to the identity of the support, although they did not use $La_2O_3$ as carrier. Our Ru La based catalysts exhibit a forward reaction rate comparable to that previously reported by other authors [18] using different supports.

### 3.2. Membrane reactor measurements

The Ru (0.6) and Ru(1.2) solids were successfully used in a membrane reactor studying the influence of the sweep gas flow rate (SG) (Fig. 2). When the SG was equal to zero, the reaction reached the theoretical equilibrium values. The $CH_4$ and the $CO_2$ conversions were 27.5 and 38.0, respectively (calculated considering both the dry reforming and the RWGS reactions). Note that with no differential pressure across the membrane, and no sweep gas flow, the reactor operated as a fixed-bed

Table 1
Reaction rates obtained over $Ru/La_2O_3$ catalysts at 823 K[a]

| Catalysts | $r_{CH_4}$ (mol $h^{-1}$ $g^{-1}$) | $r_{CH_4}$ (mol $s^{-1}$mol $Ru^{-1}$) | $r_{CO_2}$ (mol $h^{-1}$ $g^{-1}$) | $r_{CO_2}$ (mol $s^{-1}$ mol $Ru^{-1}$) | XRD[b] phases |
|---|---|---|---|---|---|
| Ru(0.2) | 0.19 | 2.7 | 0.36 | 5.2 | II-$La_2O_2CO_3$ |
| Ru(0.6) | 0.21 | 1.0 | 0.44 | 2.1 | II-$La_2O_2CO_3$ $La(OH)_3$ |
| Ru(1.2) | 0.25 | 0.6 | 0.48 | 1.1 | II-$La_2O_2CO_3$ |

[a] W/F = $4.3 \times 10^{-6}$ g h $ml^{-1}$.
[b] JCPDS: II-$La_2O_2CO_3$ (37–804), $La(OH)_3$ (36–1481 and 6–0585).

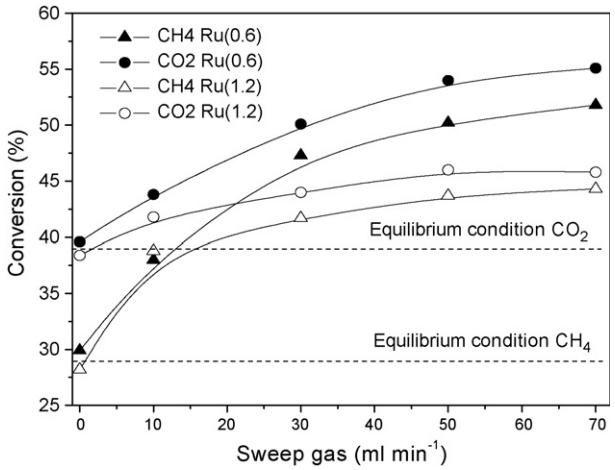


Fig. 2. Effect of SG on the performance of Ru catalysts ($T$ = 823 K, $\Delta P$ = 0 Pa, W/F = 1.03 × $10^{-3}$ g h $ml^{-1}$).

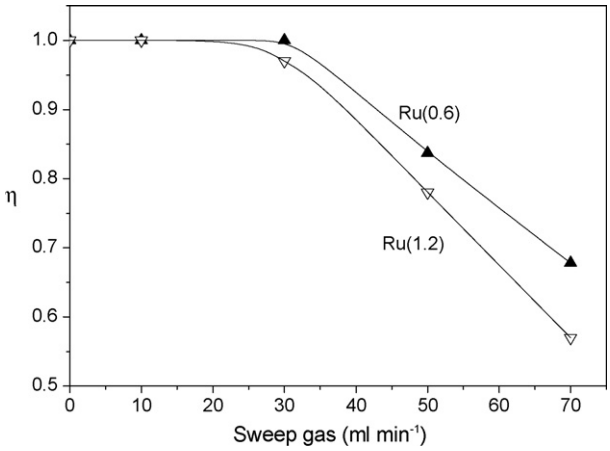


Fig. 3. Variation of the equilibration reaction ratio for the dry reforming reaction with the sweep gas flow rate. $T$ = 823 K, $\Delta P$ = 0 Pa, W/F = 1.03 × $10^{-3}$ g h $ml^{-1}$ ($\eta = \prod_i p_i^{\nu_i}/K_{eq}$).

reactor. When the SG increased, the conversions overcame those values and the difference between $CH_4$ and $CO_2$ conversions decreased. These results suggest that the hydrogen separation in the membrane reactor partially suppressed the RWGS reaction. This may be a consequence of the lower hydrogen partial pressure in the reacting zone that affects the rate of RWGS reaction. For both catalysts, the $H_2$/CO ratio was approximately 0.65 with no SG. When the SG increased, the $H_2$/CO ratio approached unity, which corresponds to the $H_2$/CO ratio for the dry reforming reaction. Both, the $CH_4$ and $CO_2$ conversions increased with the SG. In the case of the Ru(1.2) solid, both conversions reached constant values for SG higher than 30 ml $min^{-1}$. For the Ru(0.6), the conversions were higher and they steadily increased with the SG (Fig. 2).

Different approaches to describe the optimal performance of membrane reactors have been reported in the literature [19–21]. In general, it is necessary to balance the feed, reaction and permeation rates. The high activity of the catalyst is important to restore the reaction equilibrium; besides, the permeation rate should be high enough to eliminate the $H_2$ produced.

Regarding the approach to equilibrium of the dry reforming reaction [7,20,21], one can define a fraction of reaction equilibration ($\eta$) using the following equation:

$$\eta = \frac{\prod_i p_i^{\nu_i}}{K_{eq}}$$

where $p_i$ is the measured partial pressure of each reactant and product in the reaction side of the membrane reactor, $\nu_i$ the stoichiometric numbers for the $CO_2 + CH_4$ reaction, and the experimental equilibrium constant (evaluated in the fixed-bed reactor operation mode that is close to the theoretical value). If the composition corresponds to thermodynamic equilibrium, this ratio will equal 1. The $\eta$ calculated for Ru(0.6) and Ru(1.2) are shown in Fig. 3. Both catalysts can restore the equilibrium up to values of SG = 30 ml/min at which point $\eta$ begins to decrease, Ru(0.6) standing out as the most effective catalyst. Fig. 4 shows the changes in the gas composition at both sides of the membrane for Ru (0.6) and Ru (1.2) as a function of the SG. The molar fraction of CO increases on the reaction side while the molar fractions of $CO_2$, $CH_4$, $H_2$ decrease. The molar fraction of $H_2$ in the permeation side decreases due to the

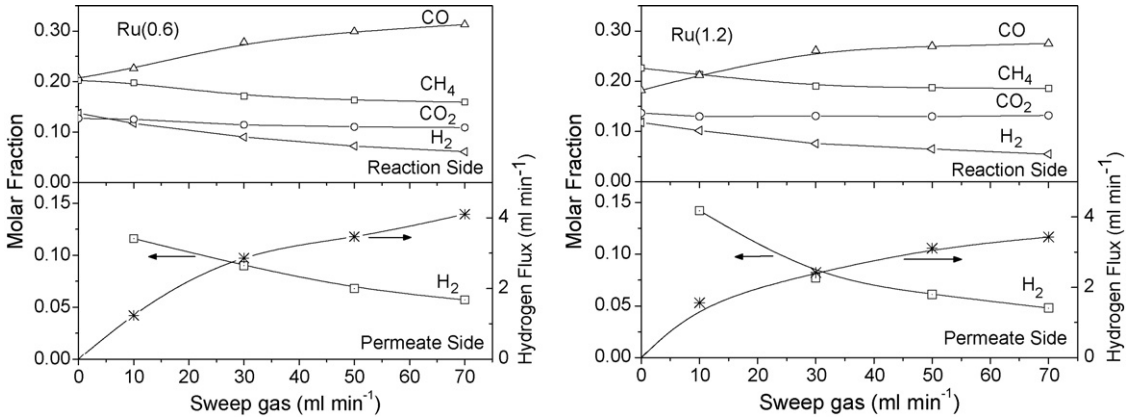


Fig. 4. Variation of the different species with the increase of the sweep gas flow rate ($T$ = 823 K, $\Delta P$ = 0 Pa, W/F = 1.03 × $10^{-3}$ g h $ml^{-1}$).

dilution effect of the SG. The membrane is 100% selective so only hydrogen is detected on the permeate side.

The increase of the Ar sweep gas flow reduces the hydrogen partial pressure on the permeate side leading to a higher $H_2$ flow rate through the membrane.

Several articles have lately appeared on membrane reactors for the methane dry reforming reaction employing different types of membranes and catalysts, such as: Pd-ceramic composite membrane and Pt, Ru, Pd, Rh, Ir/$Al_2O_3$ catalysts [6]; silica/mullite membrane ($3Al_2O_3$-$2SiO_2$) and Pt/$Al_2O_3$ catalyst [4]; Pd film supported on porous stainless steel and Ni catalysts [5]; alumina membrane with Ru deposition as catalyst [1]; $SiO_2$/alumina membrane and Rh/$Al_2O_3$ catalyst [22]. All of them report an increase in the methane conversion when extracting $H_2$ from the reaction medium, but only Lee et al. [22] and Ferreira-Aparicio et al. [5] employed a highly selective membrane. The results depend on the conditions under which the reactions were carried out such as W/F, dilution of the $CO_2 + CH_4$ mixture, membrane selectivity and its permeation capacity, carbon deposition of the catalyst which will contribute to its deactivation, etc.

It should be noticed that after each catalytic test, the membrane permeability was measured. The membrane did not show any variation on the hydrogen permeation rate and no visual damage or carbon deposition was observed. Furthermore, for all the used catalysts reported here, no carbon deposition was detected through TGA measurements. However, a small amount of graphitic carbon was detected through the much more sensitive Laser Raman spectroscopy.

### 3.3. Lanthanum phases and Ru species on calcined samples

Lanthanum oxide carbonates exist in three crystalline modifications (I, Ia and II); the three polymorphs held in an arrangement of ($La_2O_2^{2+}$) layers separated by $CO_3^{2-}$ ions. Type I has square layers and is tetragonal, while type Ia is described as a monoclinic distortion of form I [23,24]. II-$La_2O_2CO_3$ is completely indexed in the hexagonal unit cell.

In our case, the XRD patterns for all the prepared catalysts showed the presence of II-$La_2O_2CO_3$ and $La(OH)_3$ phases (Table 1). No XRD reflections associated with Ru compounds were detected.

Laser Raman spectroscopy has been reported in the literature as being used to study the oxidation of ruthenium at atmospheric pressure [25]. $RuO_2$, $RuO_4$ and $RuO_3$ have been detected upon thermal oxidation of initially reduced Ru surface. However, only a few papers have reported the application of this technique to characterize Ru supported catalysts [26].

We have previously [27] employed LRS to characterize lanthanum phases and graphitic carbon deposited during the dry reforming of methane in Rh/$La_2O_3$ catalysts. In this work, we are reporting Raman data of the Ru-lanthanum system. The Raman spectra of the Ru/$La_2O_3$ catalysts calcined at 823 K are shown in Fig. 5. The Ru(0.2) solid exhibit peaks at 358, 384, 747 and 1086 $cm^{-1}$ previously assigned to the hexagonal form of the lanthanum oxycarbonate (II-$La_2O_2CO_3$) [27]. The bands in the 350–400 $cm^{-1}$ region were assigned to La-O fundamental modes. Besides, the bands in the 700–1500 $cm^{-1}$ region correspond to the vibration of $CO_3^{2-}$ groups in the type II phase. The small signals appearing at ca. 1400 $cm^{-1}$ are due to the $\upsilon_4$ vibration of $CO_3^{2-}$. When the Ru loading increases, the oxycarbonate Raman bands become not well defined and for the Ru(1.2) catalyst, only a low-intensity signal at 384 $cm^{-1}$ could be observed. For all the solids, a broad band at 670 $cm^{-1}$ is detected that could be related to the presence of $RuO_x$ oxides.

Yan et al. [26] studied the Ru/$SiO_2$ catalyst under POM conditions using LRS. They found that the Raman spectrum recorded at 600 °C under $O_2$ showed two bands (at 489 and 609 $cm^{-1}$) attributable to $RuO_2$. These bands vanished under $H_2$ flow and reappeared when $CH_4/O_2$/Ar gases were introduced at the same temperature.

A pair of bands at 470 and 671 $cm^{-1}$ were observed in the spectrum of freshly electrodeposited Ru film [25] which were assigned to different stretching modes of hydrated $RuO_2$. The

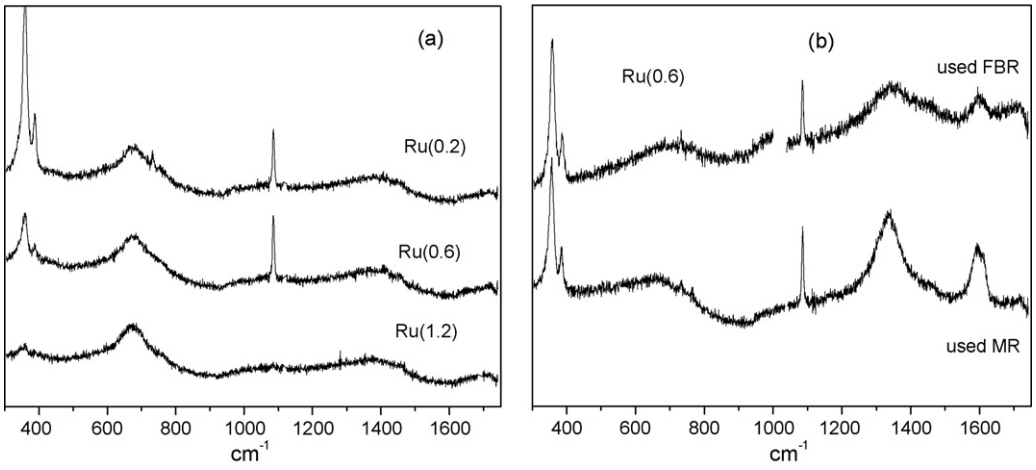


Fig. 5. Laser Raman spectra: (a) calcined Ru/$La_2O_3$ catalysts; (b) Ru(0.6) solid after $CO_2$ reforming of methane at 823 K in a fixed-bed reactor and a membrane reactor.

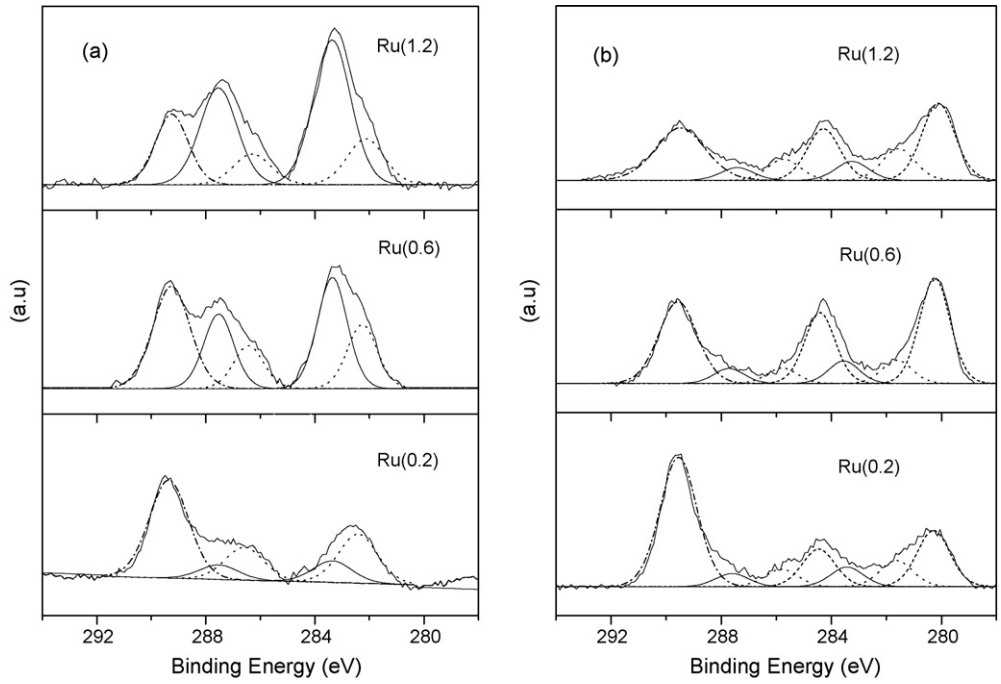


Fig. 6. Ru 3d XPS from $Ru/La_2O_3$ solids: (a) calcined and (b) used in a fixed-bed reactor. (·-·-·-·) C 1s $CO_3^{2-}$, (—) Ru(IV), (- - - -) Ru(III) and (. . .) $Ru^0$.

$RuO_3$ formation includes the appearance of an 800 $cm^{-1}$ LRS band and the presence of $RuO_4$ was deduced from the formation of an 875 $cm^{-1}$ band. In our case, no peaks were detected close to ~800 $cm^{-1}$, and only a significant broadening of the band at 670 $cm^{-1}$ was observed.

### 3.4. Surface characterization

Fig. 6 shows the Ru 3d spectra obtained on the Ru catalysts after calcination and after the $CO_2$ reforming of methane at 823 K in a fixed bed reactor. The intensity ratios and binding energies (BE) are given in Table 2. Binding energies were referenced to C 1s = 284.8 eV, which resulted in a BE for La $3d_{5/2}$ = 834.4 ± 0.2 eV for all the ruthenium solids.

There is an overlap between the Ru 3d and C 1s peaks at 284.8 eV, the latter being due to carbonaceous contamination. The C 1s spectra exhibit a well-defined peak at 289.3 eV that was attributed to carbonate carbon [15]. The low-BE C 1s peak that corresponds to the contamination carbon taken as reference was subtracted from the original spectrum. The O 1s spectra invariably showed two peaks: one at 531.2 eV was assigned to the carbonate species, and another at 528.8 eV corresponding to lattice oxygen $O^{2-}$ [28].

For the calcined solids, two Ru $3d_{5/2}$ peaks could be observed at 282.3 and 283.4 eV (Fig. 6a). According to the literature, these high-binding energy values indicate the presence of $Ru^{n+}$ species [29]. The binding energy of 284.0 eV measured in $Ru/Al_2O_3$ by several authors [29,30] was attributed to Ru(IV) species deposited onto the alumina surface.

The Ru state with a BE of 282 eV is known from the literature and has been assigned [29] to Ru(IV)/Ru(III) oxyhydrates, $Ru^{2+}$ on $Al_2O_3$, and $Ru^+$ in Y zeolite. Elmasides et al. [29] assigned this BE to an intermediate Ru oxidation state, most likely Ru(II). This state appeared to be stable on $Al_2O_3$. They [29] found that on alumina, ruthenium is incompletely reduced by treatment with $H_2$ at 823 K while on $TiO_2$, Ru is more easily reduced to the metallic state. They found that the chemical behavior depends strongly on the material on which it is supported.

In our case, the Laser Raman peak at 670 $cm^{-1}$ suggested the presence of Ru(III) species that strongly interact with La. This result is in agreement with the appearance of the 282 eV BE peak

Table 2
Binding energies and surface atomic ratio of calcined solids and after dry reforming in a fixed-bed reactor

| Samples | Treatment | C 1s $CO_3^{2-}$ (eV) | O 1s[a] (eV) | Ru/La | O/La | $C_{CO_3^{2-}}$/La | $C_{CO_3^{2-}}$/O |
|---|---|---|---|---|---|---|---|
| Ru(0.2) | Calcined | 289.3 | 531.1(88) 528.7(12) | 0.05 | 2.74 | 0.62 | 0.23 |
| | Used | 289.2 | 531.8(92) 528.7(8) | 0.06 | 2.78 | 0.78 | 0.28 |
| Ru(0.6) | Calcined | 289.5 | 531.8(89) 528.7(11) | 0.10 | 2.71 | 0.60 | 0.22 |
| | Used | 289.1 | 531.1(78) 528.8(22) | 0.12 | 3.75 | 0.89 | 0.24 |
| Ru(1.2) | Calcined | 289.4 | 531(76) 528.7(24) | 0.18 | 2.91 | 0.55 | 0.19 |
| | Used | 289.1 | 531.4(82) 528.9(18) | 0.17 | 3.63 | 0.97 | 0.26 |

[a] The relative intensity of oxygen species is given between parenthesis.

in the XPS spectra of calcined solids that could be assigned to Ru(III).The high loading catalysts have a high proportion of Ru (IV) on the surface. After being used in the fixed-bed reactor, a peak at 280.2 eV appeared (Fig. 6) that is assigned to $Ru^0$. The high BE peaks are present in low proportions.

For the used catalyst in a differential reactor, the Ru/La atomic ratio slightly changed compared to the calcined sample, suggesting that no change in the ruthenium dispersion has occurred. For all samples, dispersion values lower than 5% were obtained from CO and $H_2$ chemisorption results. The low chemisorption after a high temperature reduction is probably not indicative of the real dispersion due to the occurrence of a strong interaction between the metal and the support [15,31].

The $C_{CO_3^{2-}}$/La ratios were similar for all calcined catalysts, but increased slightly after being exposed to reaction conditions. Similarly, the $C_{CO_3^{2-}}$/O atomic ratio increased for the used sample, due to the oxycarbonate formation during reaction.

### 3.5. Reduction of Ru catalysts

Fig. 7 shows the hydrogen consumption by Ru solids as a function of temperature during the TPR experiments. For the Ru(0.2) and Ru(0.6) catalysts the profiles are similar; a small difference in the peak width can be observed. Both samples show a main reduction peak at 260 °C, a second one a 375 °C, and a low-intensity shoulder at 140 °C.

The Ru(1.2) profile is clearly different. A high intensity peak appeared at 208 °C with a significant shoulder at 260 °C while the peak at 141 °C became well defined.

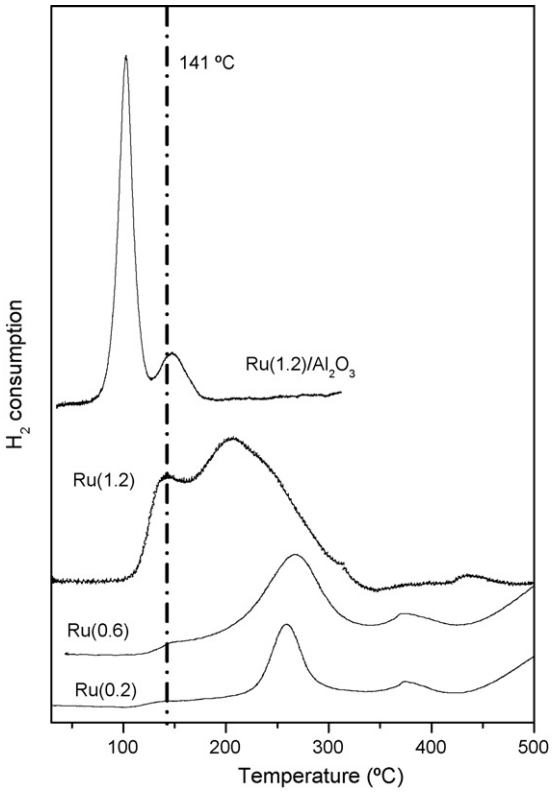


Fig. 7. TPR profiles of calcined Ru catalysts pretreated in oxygen flow at 823 K in the TPR instrument.

In previous reports [26], on $Ru/SiO_2$, the low-temperature peak (140 °C) has been assigned to the reduction of well-dispersed $RuO_x$ species and the peak at 200 °C has been attributed to $RuO_2$ particles.

From the hydrogen consumption results, the μmol $H_2$/μmol Ru ratios were calculated. For all catalysts, this ratio was close to 1.50, lower than the ratio expected for the $RuO_2$ oxide and close to the Ru(III) oxide hydrogen consumption.

The $Ru/Al_2O_3$ catalyst was prepared to help in the identification of the Ru species present on Ru/lanthanum catalysts. The TPR profile for this solid shows a sharp feature at 100 °C, followed by a low-intensity peak at 140 °C. The XRD pattern exhibits the main reflections of the monoclinic $RuO_2$ oxide. On the other hand, the Raman spectrum (not shown) only shows a very broad band centered at 600 $cm^{-1}$. Then, the low temperature TPR feature could be assigned to $RuO_2$ crystalline phase in the Ru/alumina catalyst.

The high temperature peak at 260 °C in Ru(0.2) and Ru(0.6) solids suggested the presence of a strong metal–support interaction. And the very low-intensity of the 140 °C peak is in agreement with the low dispersion of all solids.

It has been reported that Ru catalysts derived from the reduction of $RuCl_3$ retain residual chlorine following the pre-treatment in hydrogen [32]. Formation of larger metal particles (low dispersion) on samples prepared by chloride precursors has been widely reported in the literature [33].

Basinska et al. [34] have reported the presence of tetragonal LaOCl phase using select area electron diffraction in $Ru/La_2O_3$ solids calcined at 400 °C. During the impregnation procedure, chlorine was introduced and crystalline LaOCl was formed during WGS at 350 °C. However, in our solids calcined and reduced at 550 °C no oxychloride phases were detected through XRSD and LRS.

In the case of Rh La based catalysts, the strong metal–support interaction was the basis of their high stability. This strong interaction is related to the chemical affinity of Rh to form rhodates. Ru can form complex, mixed oxides with perovskite structure. However, the La–Ru perovskite phase does not crystallize at low temperature. The onset crystallization of the $LaRuO_3$ perovskite phase was found in the range of 903–927 °C [35]. Nevertheless, these temperatures depend on the method used for the preparation of the precursor.

Comparing the TPR and Raman spectroscopy results, the Raman band at 670 $cm^{-1}$ could be assigned to Ru(III) that strongly interacts with La. The presence of Ru(III) on the surface (BE peak = 282 eV) is in agreement with the bulk observations. When the Ru content is increased, the higher binding energy Ru component at 283.6 eV is proposed as arising from Ru(IV).

### 3.6. La–Ru species and carbon deposits on used samples

The XRD and Raman data of the used catalysts indicated that only the type II oxycarbonate was present, independent of the metal loading while no metallic Ru peaks were detected by XRD. For all solids, the Raman peak at 670 $cm^{-1}$ almost vanishes (Fig. 5), in agreement with the reduced state of the samples.

The Raman spectra of hexagonal crystal graphite [36,37] consists of the main first order band (G band at 1580 $cm^{-1}$) assigned to the in plane displacement of carbon atoms in the hexagonal sheets. When disorder is introduced into the graphite structure, the existing bands broaden and additional bands are found at about 1350 $cm^{-1}$ (D mode) and 1620 $cm^{-1}$ (D'mode). In the rather small or disordered crystal with very little three-dimensional order, the G and D'bands merge into a single broader feature. The G peak indicates the presence of large graphite crystals, while the ratio of the D–G peaks gives the relative amount of edge to volume of the crystals.

For the used catalysts in the fixed-bed reactor, a group of very low intensity and broad Raman bands at 1340 and 1590 $cm^{-1}$ is observed. However, for all the used catalysts reported in the present paper, no carbon deposition was detected through TGA measurements.

In the case of the catalysts used in the membrane reactor, the Raman band intensities increase, and the peaks are well defined (Fig. 5b). The same behavior has been previously reported for the $Rh/La_2O_3$ catalysts [27]. It was clearly seen that the solids evaluated at higher W/F (near the thermodynamic equilibrium) in a membrane reactor exhibited higher intensity bands due to larger amounts of graphitic carbon being formed. All catalysts were exposed to similar amounts of reactants during 180 h on stream. This phenomenon could be due to different factors; one of them may be the increase in CO concentration that favors the CO disproportionation reaction.

For these solids, the high-D/G relative intensity at low-W/F ratios indicated that the crystallization order was a function of the contact time (space velocity). The D/G ratios obtained for the Ru catalysts (D/G ∼ 4) used in a membrane reactor show that these catalysts contain a similar proportion of disordered carbon [27].

In Ru/La-based catalysts, the carbon deposits did not significantly affect the activity in the membrane reactor. This behavior could be related to the sites on which carbon is deposited and/or to the role as reaction intermediate that carbon would play.

### 3.7. Catalytic behavior and characterization results

Fig. 8 shows the $CH_4$ conversion as a function of the ratio between the permeated $H_2$ and the $H_2$ produced. Ru(0.6) presents a significant increase of methane conversion together with an effective transport of $H_2$ through the membrane.

Recently, Ferreira-Aparicio et al. [5] employed a highly selective Pd film (12–35 μm) supported on porous stainless steel and several Ni-based catalysts in a membrane reactor for the dry reforming reaction. They found that a certain $CO_2$ excess in the feed with respect to the stoichiometric ratio establishes more favorable conditions for the membrane reactor operation. Under these conditions, their system produced a hydrogen permeation flux of $4.4 \times 10^{-7}$ mol $s^{-1}$ $m^{-2}$ with a hydrogen recovery yield ($H_2$ permeate/$H_2$ produce = 0.93) of 93% for a $CO_2/CH_4$ ratio equal to 1.9 and a SG of 0.223 mmol $s^{-1}$. However, we have obtained a higher $H_2$ permeation flux equal to $5.6 \times 10^{-7}$ mol $s^{-1}$ $m^{-2}$ and a hydrogen recovery

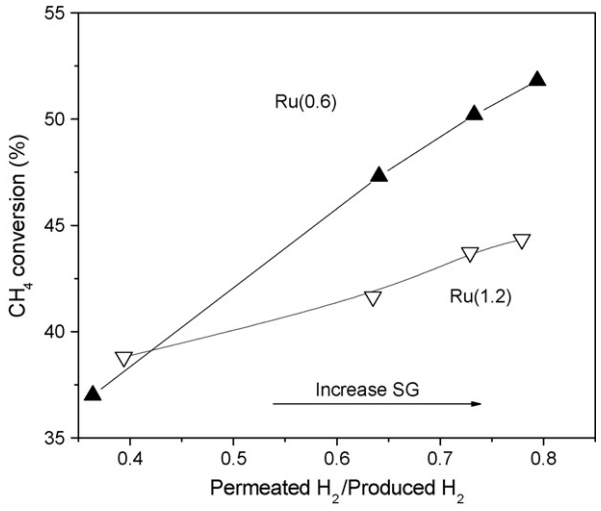


Fig. 8. Increasing sweep gas flow augments both the $CH_4$ conversion and the fraction of $H_2$ permeated ($T$ = 823 K, $\Delta P$ = 0 Pa, W/F = $1.03 \times 10^{-3}$ g h $ml^{-1}$).

of 80% employing a $CO_2/CH_4$ = 1 and a SG of 0.05 mmol $s^{-1}$ (70 ml $min^{-1}$). In both cases, a similar feed flow rate of methane (∼$3.3 \times 10^{-6}$ mol $s^{-1}$) was fed.

Of all the Ni catalysts tested by Menad and co-workers [5], the $Ni/Ce_{0.5}Zr_{0.5}O_2$ solid was the only one able to keep its surface free of carbon fibers.

Our Ru(0.6) catalyst shows higher methane conversion and hydrogen recovery than the Ru(1.2) solid. It should be noted that after 180 h on stream, the Ru(0.6) and Ru(0.2) methane conversions remain almost constant but in the case of the Ru(1.2) catalyst, the methane conversion was equal to 75% of the initial value, measured at SG of 10 ml $min^{-1}$. This low deactivation was not observed in the fixed-bed reactor. The different behavior could be assigned to the decrease in hydrogen partial pressure and the increase in CO concentration that can influence the formation of carbon deposits. In the LRS spectra for the Ru(1.2) solid, a higher ratio between the graphitic carbon bands (at 1350–1580 $cm^{-1}$) and the oxycarbonate band (at 1087 $cm^{-1}$) was observed compared to Ru(0.6) (Fig. 5).

Matsui et al. [38] have proposed the following reaction cycle for Ru/lanthanum oxide catalysts: a part of metallic Ru reacted with methane to give Ru–$CH_x$; simultaneously Ru° could be oxidized with $CO_2$ to give Ru–$O_x$ and CO, and then, oxygen transfer from Ru–$O_x$ to Ru–$CH_x$ took place to give CO and metallic Ru.

For our Ru(1.2) solids, the presence of Ru(IV) was detected through TPR experiments, which agrees with the high proportion of Ru(IV) on the surface. In this case, a fraction of the Ru loading is present as species with weaker metal–support interaction that might explain the slight deactivation of this catalyst.

## 4. Conclusions

An excellent catalyst for the $CO_2$ reforming of methane was obtained using formulations with low loadings of Ru, by far the cheapest Pt group metal. Particularly, the $Ru(0.6)/La_2O_3$

catalyst advantageously compares with the best Rh formulation that our group reported in a previous publication [7]. On the other hand, the characterization data yielded clues to understand the interplay of Ru oxidation states, varying $H_2$ partial pressures and optimal Ru concentration with the slight deactivation observed when the Ru(1.2) formulation was used in the membrane reactor. These statements are supported by the following observations:

- For the most effective catalyst, Ru(0.6), we obtained a high $H_2$ permeation flux ($5.6 \times 10^{-7}$ mol $s^{-1}$ $m^{-2}$) and a hydrogen recovery of 80% compared with $3.1 \times 10^{-7}$ mol $s^{-1}$ $m^{-2}$ for Rh(0.6)/$La_2O_3$-$SiO_2$, employing in both cases a $CO_2$/$CH_4$ = 1 and a SG flow rate of 0.05 mmol $s^{-1}$ (70 ml $min^{-1}$).
- Through the TPR and Raman spectroscopy data, the Raman band at 670 $cm^{-1}$ could be assigned to Ru(III) that strongly interacts with La. The presence of Ru(III) on the surface (BE peak = 282 eV) is in agreement with the bulk observations.
- Although all the catalysts were stable in the fixed bed-reactor, a slight deactivation was observed for the Ru(1.2) formulation in the membrane reactor. This behavior could be assigned to the decrease in hydrogen partial pressure and the increase in CO concentration during membrane reactor operation.
- A higher proportion of graphitic carbon detected in the Ru(1.2) solid is in agreement with the decrease in methane conversion, which could be related to the presence of Ru(IV) detected through the TPR experiments.

## Acknowledgements

The authors wish to acknowledge the financial support received from UNL, CONICET and ANPCyT. They are also grateful to the Japan International Cooperation Agency (JICA) for the donation of the major instruments used in this study. Thanks are also given to Prof. Elsa Grimaldi for the edition of the English paper and to Prof. Patricio Ruiz and Pierre Eloy for the XPS analysis.

## References

[1] L. Paturzo, F. Galluci, A. Basile, G. Vitulli, P. Pertici, Catal. Today 82 (2003) 57.
[2] A.K. Prabhu, R. Radhakrishnan, S. Ted Oyama, Appl. Catal. A: Gen. 183 (1999) 241.
[3] B.S. Liu, C.T. Au, Catal. Lett. 77 (2001) 67.
[4] P. Ferreira-Aparicio, I. Rodríguez-Ramos, A. Guerrero-Ruiz, Appl. Catal. A: Gen. 237 (2002) 239.
[5] P. Ferreira-Aparicio, M. Benito, S. Menad, J. Catal. 231 (2005) 331–343.
[6] E.Y. Kikuchi, Chen. Stud. Surf. Sci. Catal. 107 (1997) 547.
[7] S. Irusta, J. Múnera, C. Carrara, E.A. Lombardo, L.M. Cornaglia, Appl. Catal. A 287 (2005) 147–158.
[8] R. Hughes, Membr. Technol. 131 (2001) 9.
[9] P. Ciaverella, D. Casanave, H. Moueddeb, S. Miachon, K. Fiaty, J.-A. Dalmon, Catal. Today 67 (2001) 177.
[10] M. Bradford, M. Vannice, Catal. Rev. Sci. Eng. 41 (1999) 1.
[11] K. Nagaoka, M. Okamura, K. Aika, Catal. Commun. 2 (2001) 255.
[12] F. Mark, W. Maier, J. Catal. 164 (1996) 122.
[13] P. Ferreira-Aparicio, L. Rodriguez-Ramos, J.A. Anderson, A. Guerrero-Ruiz, Appl. Catal. A: Gen. 202 (2000) 183.
[14] S. Irusta, L. Cornaglia, E. Lombardo, J. Catal. 210 (2002) 7.
[15] G. Gallaher, J. Goodwin, C. Huang, M. Houalla, J. Catal. 140 (1993) 453.
[16] U.L. Portugal, C.M. Marques, E.C. Araujo, E.V. Morales, M.V. Giotto, J.M.C. Bueno, Appl. Catal. A: Gen. 193 (2000) 173.
[17] M. Bradford, M.A. Vannice, J. Catal. 183 (1999) 69.
[18] J. Wei, E. Iglesia, J. Phys Chem. B 108 (2004) 7253.
[19] C. Reo, L. Bernstein, C. Lund, Chem. Eng. Sci. 52 (1997) 3075.
[20] L. Li, R. Borry, E. Iglesia, Chem. Eng. Sci. 57 (2002) 4595.
[21] S. Ma, C. Lund, Ind. Eng. Chem. Res. 42 (2003) 711.
[22] D. Lee, P. Hacarlioglu, S.T. Oyama, Top. Catal. 29 (2004) 45–57.
[23] R. Taylor, G. Schrader, Ind. Eng. Chem. Res. 30 (1991) 1016.
[24] R. Turcotte, J. Sawyer, L. Eyring, Inorg. Chem. 8 (1969) 238.
[25] H. Chan, C.G. Takoudis, M.J. Weaver, J. Catal. 172 (1997) 336.
[26] G.G. Yan, T. Wu, W. Weng, H. Toghiani, R.K. Toghiani, H.L. Wan, C.U. Pittman, J. Catal. 226 (2004) 247.
[27] L. Cornaglia, J. Múnera, S. Irusta, E. Lombardo, Appl. Catal. A: Gral. 263 (2004) 91.
[28] S. Lacombe, C. Geantet, C. Mirodatos, J. Catal. 151 (1994) 439.
[29] C. Elmasides, D.I. Kondarides, W. Grünert, X.E. Verykios, J. Phys. Chem. B 103 (1999) 5227.
[30] E. Tsisum, B. Nefedov, E. Shpiro, G. Antoshin, K. Minachev, React. Kinet. Catal. Lett. 24 (1984) 37.
[31] S. Chan, A. Bell, J. Catal. 89 (1984) 433.
[32] P.G. Koopman, A.P.G. Kieboom, H. Van Bekkum, J. Catal. 69 (1981) 172.
[33] C. Crisafulli, S. Scire, R. Maggiore, S. Minico, S. Galvagno, Catal. Lett. 59 (1999) 21.
[34] A. Basinska, L. Kepinski, F. Domka, Appl. Catal. A: Gen. 183 (1999) 143.
[35] Nitin K. Labhsetwar, V. Balek, E. Večerníková, P. Bezdička, J. Subrt, T. Mitsuhashi, S. Kagne, S. Rayalu, H. Haneda, J. Colloid Interface Sci. 300 (2006) 232.
[36] Y. Wang, D.C. Alsemeyer, R. Mc Creery, Chem. Mater. 2 (1990) 557.
[37] T. Reshetenko, L. Avdeeva, Z. Ismagilov, V. Pushkarev, S. Cherepanova, A. Chuvilin, V. Likholobov, Carbon 41 (2003) 1605.
[38] N. Matsui, K. Anzai, N. Akamatsu, K. Nakagawa, N. Ikenaga, T. Suzuki, Appl. Catal. A: Gen. 179 (1999) 247.